Measurements of the Rate Constant of $HO_2 + NO_2 + N_2 \rightarrow HO_2NO_2 + N_2$ Using Near-Infrared Wavelength-Modulation Spectroscopy and UV−Visible Absorption Spectroscopy

Lance E. Christensen*,† and Mitchio Okumura*

Arthur Amos Noyes Laboratory of Chemical Physics, Division of Chemistry and Chemical Physics, California Institute of Technology, Pasadena, California 91125

Stanley P. Sander,* Randall R. Friedl, and Charles E. Miller

Jet Propulsion Laboratory, California Institute of Technology, Pasadena, California 91109

James J. Sloan

Department of Chemistry, University of Waterloo, Waterloo, Ontario N2L 3G1, Canada

Received: July 2, 2003; In Final Form: October 21, 2003

Rate coefficients for the reaction $HO_2 + NO_2 + N_2 \rightarrow HO_2NO_2 + N_2$ (reaction 1) were measured using simultaneous near-IR and UV spectroscopy from 220 to 298 K and from 45 to 200 Torr. Using the data acquired in the present experiment, the low-pressure and high-pressure limit rate constants for reaction 1 were determined to be $k_o = (2.1 \pm 0.1) \times 10^{-31} \times (T/300)^{-(3.1\pm0.3)}$ cm^6 molecule^{-2} s^{-1} and $k_\infty = (2.4 \pm 0.1) \times 10^{-12} \times (T/300))^{-(1.9\pm0.5)}$ cm^3 molecule^{-1} s^{-1}, using the expressions for rate constants adopted by the NASA data evaluation panel ($F_c = 0.6$). The reaction rate was significantly enhanced in the presence of methanol due to a chaperone effect involving an $HO_2 \cdot CH_3OH$ complex. Enhancement parameters for this process were quantified as a function of temperature. During the course of our studies, we observed an unexpected time-dependent UV absorption unaccounted for in previous examinations of reaction 1 that employed UV spectroscopy to monitor HO_2. We show that this absorption, which may have led to errors in those prior studies, is due to the process $NO_2 + NO_2 \rightleftarrows N_2O_4$ (reaction 3). Using UV−visible spectroscopy, we determine k_{-3} to be (36 ± 10) s^{-1} at 231 K and 100 Torr using the NASA-recommended equilibrium constant for the dimerization of NO_2. This represents the first measurement of k_{-3} at $T < 250$ K.

I. Introduction

The reaction between HO_2 and NO_2 has been the subject of numerous laboratory studies[1−10] and has been shown to be a recombination reaction which forms peroxynitric acid, HO_2NO_2:

$$HO_2 + NO_2 \xrightarrow{M} HO_2NO_2 \qquad (1)$$

A bimolecular channel has also been suggested,[11] but it appears to be insignificant in comparison with reaction 1. Reaction 1 plays an important role in the atmosphere. The reaction couples the NO_x and HO_x chemical families, and the subsequent reaction of HO_2NO_2 with OH is an important sink of HO_x in the upper troposphere and lower stratosphere.[12] Measurements of HO_2-NO_2 from space[13] and balloon-borne[14] platforms have enabled researchers to test our understanding of atmospheric processes involving HO_2NO_2. Recently, it has been shown that photolysis of HO_2NO_2 is an important source of HO_x under high-latitude, high solar zenith angle conditions.[15] Accurate measurements of $k_1(M,T)$, the effective bimolecular rate coefficient for the termolecular reaction 1, are thus necessary to predict HO_2NO_2 concentrations and correctly describe the chemistry of this region of the atmosphere.

Recent experiments in our laboratory have raised questions about reported rate coefficients of reactions of HO_2 at low temperatures.[16] Current recommendations[17,18] for the rate coefficient of reaction 1 have relied heavily on studies that utilized methanol as a precursor for HO_2. However, we have shown that for the reaction

$$HO_2 + HO_2 \rightarrow H_2O_2 + O_2 \qquad (2)$$

the typical methanol concentrations employed for kinetic studies of reaction 2 ($\sim 10^{15}$ molecules cm^{-3}) cause a significant enhancement of the observed rate for temperatures below 250 K.[16] Although the enhancement of HO_2 reaction rates in the presence of hydrogen bonding species has been observed for over two decades,[19−23] most previous studies of HO_2 reactions using methanol as a precursor neglected this effect. If reaction 1 were similarly enhanced, then currently recommended rates would be too high at temperatures below 250 K.

In addition, the studies of reaction 1 that have had the greatest influence on current recommendations failed to account for the effect of N_2O_4 formation/dissociation at temperatures below 250 K on measurements of k_1.[8−10] These studies employed UV spectroscopy of HO_2 between 225 and 230 nm due to the strong absorption of HO_2 in this spectral region. However, NO_2 and

* Authors to whom correspondence should be addressed. E-mail: (Christensen) lance.christensen@jpl.nasa.gov; (Sander) stanley.sander@jpl.nasa.gov; (Okumura) mo@its.caltech.edu.

† Present address: Jet Propulsion Laboratory, California Institute of Technology, Pasadena, CA.

10.1021/jp035905o CCC: $27.50
Published on Web 12/05/2003

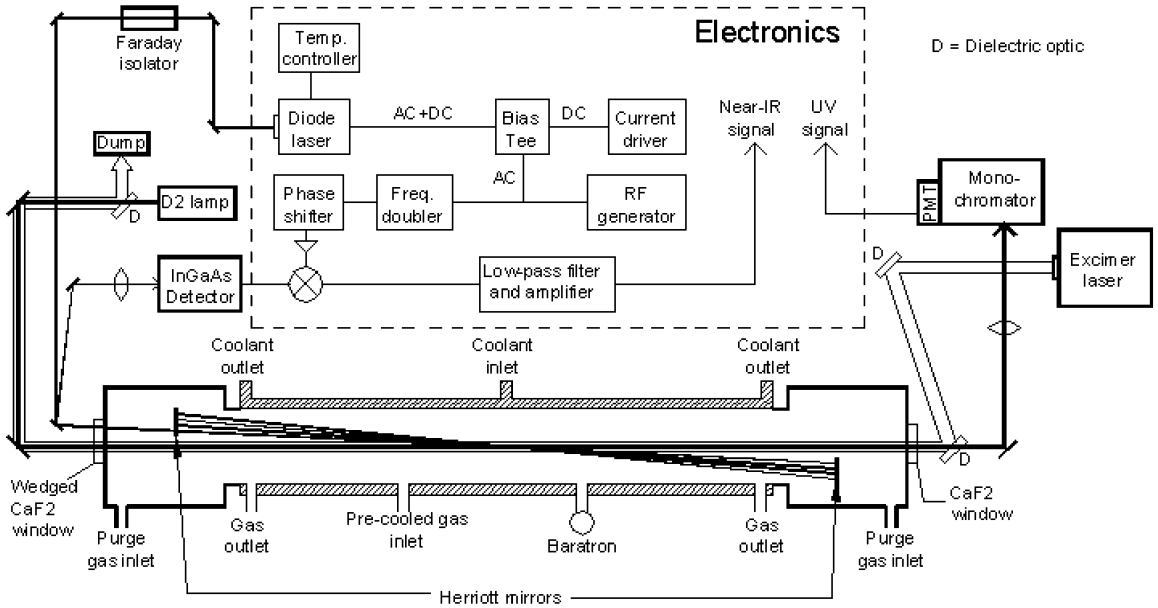

Figure 1. Experimental apparatus. The UV and near-IR probes entered the reaction cell from the opposite direction as the excimer pulse. Not depicted are the 30 passes of the near-IR beam between the Herriott mirrors.

N_2O_4 also absorb significantly at these wavelengths. At low temperatures, the formation of N_2O_4 via the equilibrium process

$$NO_2 + NO_2 \rightleftarrows N_2O_4 \qquad (3)$$

becomes significant. In typical laboratory studies of reaction 1, the HO_2 that is produced by flash photolysis quickly depletes a small fraction of the NO_2 and the equilibrium between NO_2 and N_2O_4 is perturbed. As the system relaxes back to equilibrium, NO_2 is formed and N_2O_4 is lost. Since both these species absorb in the UV, the time dependence of the UV signal is altered. It will be shown below that this has likely affected previous kinetic studies of $HO_2 + NO_2$.

The problem of overlapping absorptions in the UV can be overcome by monitoring HO_2 in the near-IR. The first overtone band of the OH stretch as well as bound-to-bound transitions to the low-lying electronic state of HO_2 are accessible to tunable near-infrared diode lasers. These bands[24−26] consist of isolated rovibronic or rovibrational lines that allow for unambiguous detection using high-resolution methods. The use of diode lasers also permits the employment of heterodyne detection techniques. Previous researchers have demonstrated the benefits of diode-laser heterodyne detection in the near-infrared for the study of HO_2 kinetics[27] and spectroscopy.[25] Heterodyne detection using diode lasers enables the measurement of fractional absorbances on the order of 1×10^{-6} in a 1 Hz bandwidth.[28] This level of detection far surpasses that obtainable by direct absorbance measurements in the UV. In the present study, we employed heterodyne techniques in the lower MHz range (wavelength-modulation spectroscopy) to improve the signal-to-noise of the near-IR channel.

In this work, we have reexamined the reaction between HO_2 and NO_2 using UV spectroscopy to monitor NO_2, and near-IR wavelength-modulation spectroscopy to monitor HO_2. We found a significant enhancement by methanol on the overall rate of $HO_2 + NO_2$. The rate coefficient at zero methanol, k_1, was determined by measuring the overall rate at different methanol concentrations and extrapolating to zero methanol. The rate coefficient k_1 was measured over the temperature range 220 K to 298 K and pressure range 40 Torr to 200 Torr. We performed additional experiments using the UV probe to monitor total absorbance at several different wavelengths. These experiments demonstrated that N_2O_4 association and dissociation could interfere with kinetic measurements of reaction 1 in the UV and may have adversely affected previous determinations of k_1.

II. Experimental Section

A. Apparatus. Figure 1 is a schematic diagram of the experimental apparatus. The reaction was studied in a temperature-controlled flow cell. A XeCl pulsed excimer laser (308 nm) photolyzed either F_2 or Cl_2, initiating reactions that formed HO_2 in excess NO_2. The NO_2 concentration was monitored with UV−visible direct absorption spectroscopy. The concentration of HO_2 was monitored with heterodyne spectroscopy using a near-IR diode laser. Near-IR and UV measurements were done simultaneously.

The reaction cell was a 175 cm long, 5 cm diameter Pyrex cylinder supported at each end by aluminum chambers. The cell was surrounded by an insulated jacket through which flowed methanol chilled by a liquid-nitrogen cooled heat exchanger. Thermocouples located inside the reaction cell allowed the temperature to be measured to within ±1 K. Reagent gases were cooled in a meter-long mixing tube prior to entering the main reaction cell. They entered from the middle of the main reaction cell and flowed toward the outlet ports.

N_2 confinement gas flowing from both aluminum chambers restricted the reactants to a region 137 ± 1 cm long between the outlet ports. To test the extent of confinement, gas mixtures containing known amounts of Cl_2 and NO_2 were flowed through the reagent entrance port. The UV absorbances due to Cl_2 and NO_2 were measured and the effective path length was calculated using Beer's Law analysis and tabulated absorption cross sections.[17] These tests were conducted over the range of pressures and flow rates utilized in the experiment. They confirmed that the reagent gases were contained between the two exit ports with an effective path length matching the separation between the centerlines of the two ports to within 1 cm.

The extent of confinement was further verified by comparing rate measurements of reactions 1 and 2 acquired with and without the use of confinement gas. In the latter scheme, reagent

gas was present throughout the reaction cell. The path length for the UV analysis beam was then simply the distance between the entrance and exit windows. Rate constant measurements for these two schemes agreed to within 5%.

The excimer photolysis pulse entered the cell through a CaF_2 window on one of the aluminum chambers. The 20 ns pulses had a 2 cm × 1 cm rectangular cross section. The pulse energy ranged from 60 mJ to 150 mJ. The pulses passed through the middle of the cell, creating a 2 cm × 1 cm × 137 cm photolysis region. The excimer laser was configured as an unstable optical resonator to minimize the divergence of the photolysis beam.

The photolysis volume, defined as the overlap region between the reagents and the photolysis pulse, was centrally located within the reaction cell, thus minimizing the effect of wall reactions on the HO_2 disappearance rate. However, transport of reactive species from the photolysis volume into the surrounding gas by turbulent mixing was an important consideration. To test this effect, the $C_2H_5O_2$ and HO_2 self-reactions were studied at $[C_2H_5O_2]_o < 1 \times 10^{13}$ molecules cm^{-3} and $[HO_2]_o < 5 \times 10^{11}$ molecules cm^{-3}, respectively. $C_2H_5O_2$ was formed from the photolysis of Cl_2 in the presence of ethane and oxygen. At these low concentrations, the calculated chemical loss rates for both species were less than 2 s^{-1}; consequently, other loss processes, such as turbulent mixing and diffusion, became comparable. It was observed that as the residence time was increased, observed rates of $C_2H_5O_2$ and HO_2 loss decreased asymptotically toward the predicted chemical loss rates. This indicated that turbulent mixing was more dominant than diffusion as a loss process for species formed within the photolysis volume. The measured first-order loss due to turbulent mixing was 2−4 s^{-1} for a residence time of 15 s at 298 K for both the near-IR and UV channels. Turbulent mixing effects decreased with decreasing temperature. The residence time was adjusted to ensure that turbulent mixing had less than a 5% effect on measured rate coefficients.

Calibrated flows of reagent gases were mixed prior to entering the cell. Flow conditions were adjusted so that the cell residence time was 3−10 s, approximately equal to the interval between photolysis laser pulses. HO_2 was formed from the reaction sequence

$$Cl_2 \xrightarrow{h\nu} 2Cl \quad (4)$$

$$Cl + CH_3OH \rightarrow HCl + CH_2OH \quad (5)$$

$$CH_2OH + O_2 \rightarrow HO_2 + CH_2O \quad (6)$$

The concentrations (molecules cm^{-3}) of the reagents were Cl_2: (2−6) × 10^{15}; He: (2−5) × 10^{16}; CH_3OH: (1−3) × 10^{14} (measurements of k_1 at low $[CH_3OH]$) or (5−80) × 10^{15} (for parametrization of methanol effect—see below); O_2: (2−7) × 10^{17}; NO_2: (6−50) × 10^{14}. The buffer gas was N_2 for all experiments. The range of $[HO_2]_o$ was (5−8) × 10^{13} molecules cm^{-3}. The Cl_2 and He came from a mixed cylinder of 10.0% Cl_2 (99.5% purity) in He (99.999%). N_2 (99.9993%) was bubbled through CH_3OH (A.C.S. Reagent Grade) in a temperature-controlled saturator to obtain the desired gas-phase methanol concentration. NO_2 was prepared by mixing NO (99% purity) with a large excess of O_2 (99.996%) and allowing the mixture to stand for a day. All gases were acquired from Air Products and Chemicals, Inc. except NO, which was acquired from Matheson Tri-Gas, Inc.

Important Note: An attempt was made to study reaction 1 using the photolysis of $F_2-H_2-O_2$ mixtures to produce HO_2. When NO_2 was added to a mixture consisting of (molecules cm^{-3}) $[F_2] = 5 \times 10^{16}$, $[H_2] = 5 \times 10^{16}$, $[O_2] = 5 \times 10^{17}$, and balance N_2 (100 Torr) at 231 K, the mixture spontaneously decomposed in the reaction cell, resulting in a small explosion. No further experiments were carried out using $F_2-H_2-O_2-NO_2$ mixtures. Other methods of producing HO_2 were considered but not utilized: $Cl_2-H_2-O_2$ would produce HO_2 too slowly and in amounts too small (H_2 has to compete with NO_2 for Cl atoms) and $Cl_2-CH_2O-O_2$ photolysis might be complicated by complexation between CH_2O and HO_2.

TABLE 1: UV and Visible Cross Sections for Various Species at 298 K[a]

	wavelengths				
species	220 nm	369.50 nm	381.875 nm	400 nm	ref
HO_2	3.41				NASA[17]
NO_2	0.40	0.523[b]	0.562[c]	0.60	Bass et al.[39]
N_2O_4	6.68	0.167			Bass et al.[39]
HO_2NO_2	1.18				NASA[17]

[a] In units of 10^{-18} cm^2; blank spaces indicate that the cross-section is less than 5% of the cross-section of NO_2 at a particular wavelength. [b] T dependence of -1.1×10^{-22} cm^2 K^{-1}, from Davidson et al.[34] [c] T dependence of -8.7×10^{-23} cm^2 K^{-1}, from Davidson et al.[34]

B. UV Detection. The source of UV light was a 150 W, D_2 lamp (Hamamatsu). The UV probe beam was coaligned with the photolysis beam, made one pass through the photolysis volume, and was reflected by a dichroic mirror and focused onto the entrance slit of a monochromator (Acton SpectraPro 300i). A photomultiplier tube (PMT) was mounted at the exit slit. Baffles in both aluminum chambers ensured that only UV light that had sampled the photolysis volume entered the monochromator. The UV probe beam entered the apparatus through a 30′ wedged CaF_2 window on the aluminum chamber opposite the input aluminum chamber for the photolysis beam. Because the 308 nm excimer light could not be completely rejected, the UV measurements typically began 400 μs after the photolysis pulse, to allow time for the PMT and electronics to recover.

To monitor the concentration of NO_2, the monochromator was set to 369.500 nm for experiments conducted at temperatures of 230 K and higher. At lower temperatures, the monochromator was set to 381.875 nm to minimize interference from N_2O_4. The cross-sections of NO_2, N_2O_4, HO_2, and HO_2NO_2 are listed in Table 1. Contributions to the total absorbance at 368.500 and 381.875 nm from HO_2, H_2O_2, HO_2NO_2, and Cl_2 were less than 2% at all temperatures. At temperatures below 250 K, a significant fraction of NO_2 dimerized to N_2O_4. At 219 K, $[N_2O_4]/[NO_2]$ reached values as high as 0.8. To maintain the contribution of N_2O_4 to the total absorbance to less than 5%, NO_2 was monitored at 381.875 nm for experiments below 230 K. The cross-sections at 308 nm for NO_2 and N_2O_4 were 1.6×10^{-19} and 2.9×10^{-19}, respectively.[39]

C. Near-IR Detection. The near-IR source was a 3 mW distributed-feedback (DFB), continuous-wave, tunable diode laser manufactured by the JPL Microdevices Laboratory. The diode laser frequency could be varied between 6620 cm^{-1} and 6645 cm^{-1} by adjusting the bias current and laser temperature. The line width (fwhm) of the emission was approximately 20 MHz as determined by deconvolving spectra of H_2O transitions at pressures below 500 mTorr.

For the present study, an HO_2 transition at 6638.2 cm^{-1} was probed. This line is assigned to the $^qQ_2$ transition (a band head) of the first overtone of the O−H stretch.[29] Another diode laser that emitted near 7000 cm^{-1} (JPL Microdevices Laboratory) was also employed in the experiment but only for a limited

number of experiments at room temperature. This second diode laser probed transitions to the low-lying electronic state of HO_2 ($^2A' \leftarrow {}^2A''$). No significant differences in measured kinetic parameters were observed between the two lasers. The cross-section of the $^qQ_2$ line at 100 Torr, 298 K was estimated to be $(4 \pm 2) \times 10^{-20}$ cm^2. This was determined by comparison to other HO_2 transitions near 6627 cm^{-1} in which cross sections have been previously determined.[25]

Like the UV beam, the near-IR beam entered the apparatus through the 30′ wedged CaF_2 window on the aluminum chamber opposite that of the excimer input. After passing through the CaF_2 window, the beam passed through a small opening in a gold-coated mirror with a 2032 mm radius of curvature and impinged on a similar mirror in the other aluminum chamber positioned 1820 mm from the input mirror. These two mirrors formed a Herriott cell[30,31] that folded the beam, resulting in 30 passes through the photolysis volume. The beam was inside the photolysis volume for approximately half the length of a single pass between mirrors. The effective path length of the near-IR beam was approximately 2700 cm by visual inspection. This was maximized by placing the Herriott mirrors as close to the path of the excimer pulse as possible.

The laser current was modulated at 6.80 MHz through an external bias tee. The signal from the InGaAs photodiode detector was demodulated at 13.6 MHz (2f detection) and low-pass filtered, generally between 3 kHz and 10 kHz. These bandwidths were more than a factor of 5 larger than the HO_2 loss rate. Minor adjustments of the amplitude of modulation were required to optimize the signal when the pressure and temperature of the cell were varied. The measured HO_2 detection sensitivity was approximately 8×10^{-10} cm^{-1} in a 1 Hz bandwidth. At the highest concentration of HO_2 employed in the present experiment, 8×10^{13} molecules cm^{-3}, the absorbance was observed to be less than 0.01. Thus, the heterodyne signal for $[HO_2]$ deviated from Beer's law by less than 1% under all conditions.

D. Calibration and Comparison of UV and Near-IR Probes. The kinetics of reaction 1 were studied under first-order conditions, which eliminated the need for absolute calibration of the HO_2 near-IR signal. However, calibration was necessary to correctly model the reaction conditions and account for secondary processes. Also, while the near-IR and UV beams overlapped significantly, they had different geometric paths, and did not probe identical regions of the photolysis volume. Both issues were addressed by measuring the kinetics for the HO_2 self-reaction with simultaneous detection of HO_2 by the two spectral channels. If the near-IR and UV probes gave identical bimolecular kinetics, then we could show that the conditions sampled by the two beams were the same. Once this correspondence was established, a comparison of the rate coefficients acquired by each channel allowed us to calibrate the near-IR signal, since the cross-section and path length for the UV absorption by HO_2 is known.

Our tests of the HO_2 self-reaction followed the procedures of our previous experiments.[16] To prevent complications from $HO_2 \cdot CH_3OH$ complex formation in the $Cl_2-CH_3OH-O_2$ system, we generated HO_2 by photolysis of F_2 in $H_2-O_2-N_2$ gas mixtures. The HO_2 self-reaction is second-order and for both probe beams, the observed signal can be described by the equation

$$Sig(t) = -b + \left(\frac{1}{Sig_o + b} + 2kt\right)^{-1} \qquad (7)$$

where $Sig(t)$ is the signal as a function of time, Sig_o represents the signal at time = 0, b represents a constant baseline offset, and k represents the second-order rate constant in units of Sig^{-1} s^{-1}. For UV measurements, $Sig(t)$ was in units of absorbance (dimensionless). For near-IR measurements, $Sig(t)$ was in units of volts. For the present experiment, the value of k from the UV measurements was corrected for the contribution of H_2O_2 by multiplying its value by $1 - (\sigma_{H_2O_2}/2\sigma_{HO_2})$, following the procedure outlined by Kircher and Sander.[32]

If the only differences between the two independent probes are the units in which the signals are measured, the product $k \times Sig_o$ (in units of s^{-1}) is the same for both channels regardless of differences in path length or cross-section. This product is equivalent to the instantaneous first-order loss rate extrapolated back to time zero. In the present experiment, this was observed to be true under all conditions. Thus, we concluded that the two probe beams measured the same physical processes identically.

Because the UV cross section and the path length were known, the UV measurement allowed us to measure the absolute concentration of HO_2, and hence provided a second-order rate constant in units of cm^3 molecule^{-1} s^{-1}. The near-IR probe measured a second-order rate constant in units of V^{-1} s^{-1}. The ratio of the rate constants gave the scaling factor used to convert the near-IR signal from units of volts to molecules cm^{-3}. This value ranged between $(1-6) \times 10^{16}$ molecules V^{-1} at the RF port of the demodulation mixer.

E. Analysis of Secondary Reactions. To determine rate constants for reaction 1, the effects of several secondary reactions were considered. The most significant of these was the HO_2 self-reaction. As in previous studies of reaction 1,[8-10] HO_2 was generated in excess NO_2 and the decay of HO_2 was analyzed using first-order rate analysis. The HO_2 self-reaction contributed an additional second-order loss process. As shown in previous studies,[9] the effect of the HO_2 self-reaction on the determination of the pseudo-first-order rate coefficient, k', varies little with the concentration of NO_2. Therefore, k_1 can be determined from $dk'/d[NO_2]$. To verify this, three tests were done. First, kinetic modeling using FACSIMILE[33] was used to determine the effect of the HO_2 self-reaction on the overall rate measurement of k_1. The reactions considered in the model are listed in Table 2. The HO_2 self-reaction affected the determination of k_1 by less than 3% under most conditions. The largest correction to k_1 was a 6% decrease in the value observed at 50 Torr and 298 K. At 100 Torr, the correction was less than 3% for all temperatures. Second, we observed that measured k_1 values did not differ by more than 5% when $[HO_2]_o$ was varied over an order of magnitude. Third, no significant difference in the value of k_1 was observed when fits were conducted over

TABLE 2: Reactions Used for Kinetic Modeling[a]

# in text	reaction	rate
5	$Cl + CH_3OH \rightarrow HCl + CH_2OH$	ref 17
6	$CH_2OH + O_2 \rightarrow HO_2 + CH_2O$	ref 17
2	$HO_2 + HO_2 \rightarrow H_2O_2 + O_2$	ref 16
8	$NO + HO_2 \rightarrow NO_2 + OH$	ref 17
not listed	$OH + NO_2 + M \rightarrow HNO_3 + M$	ref 17
not listed	$OH + HO_2 \rightarrow H_2O + O_2$	ref 17
not listed	$Cl + HO_2 \rightarrow HCl + O_2$	ref 17
1	$HO_2 + NO_2 + M \rightarrow HO_2NO_2 + M$	ref 17
not listed	$Cl + NO_2 + M \rightarrow ClONO + M$	ref 17
not listed	$Cl + NO_2 + M \rightarrow ClNO_2 + M$	ref 17
not listed	$Cl + ClONO \rightarrow Cl_2 + NO_2$	ref 17
not listed	$Cl + ClNO_2 \rightarrow Cl_2 + NO_2$	ref 17
3,−3	$NO_2 + NO_2 \leftrightarrow N_2O_4$	ref 17
−3	$N_2O_4 + M \rightarrow NO_2 + NO_2 + M$	36 s^{-1} [b]

[a] Used only for qualitative analysis. [b] At 231 K, 100 Torr.

different time intervals. The influence of the HO_2 self-reaction should be the largest at earlier times.

Another potential complication in the analysis is the effect of NO_2 photolysis by the excimer laser. NO produced from NO_2 photolysis can affect the measured HO_2 decay rate because of the reaction

$$HO_2 + NO \rightarrow OH + NO_2 \quad (8)$$

To assess the magnitude of the kinetic interference from reaction 8, it was necessary to determine the fractional NO_2 decomposition by the photolysis laser at 308 nm. This was obtained by photolyzing NO_2 in the presence of O_2 and measuring the O_3 formed using UV absorption at 255 nm. In this way, the fractional NO_2 photodecomposition at a laser pulse energy of 100 mJ was found to be $(2.8 \pm 0.2) \times 10^{-3}$. Davidson et al.[34] have shown that at 219 K, the NO_2 cross-section at 308 nm is only 2% higher than at room temperature, indicating that the fraction of NO_2 dissociated by photolysis was approximately the same at all temperatures. Kinetic modeling indicated that at 50 Torr and 295 K, the effect of NO formation would be to increase k_1 by 6%. At higher pressures and lower temperatures, the effect of NO diminishes. The observed rate was influenced by less than 3% at all other temperatures and pressures examined in the present experiment. Measurements in the present study have taken this correction into account.

Possible complications arising from the formation of ClONO and $ClNO_2$ via the reaction of Cl with NO_2 were considered. ClONO and $ClNO_2$ are produced via the reaction $Cl + NO_2 + M$. At $[CH_3OH] = 4 \times 10^{15}$ molecules cm^{-3} and $[NO_2] = 2.9 \times 10^{15}$ molecules cm^{-3}, the fraction of Cl that reacts with NO_2 as opposed to CH_3OH is approximately 0.2 at 231 K and 100 Torr, according to the NASA recommended rate coefficients for these reactions. Determinations of the time dependence of HO_2 would be affected if ClONO or $ClNO_2$ were to react appreciably with HO_2. To address this issue, k_1 was measured in the near-IR as a function of $[Cl]_o$ at constant $[CH_3OH]$. The value of k_1 was found to be independent of $[Cl]_o$ over an order of magnitude change in $[Cl]_o$ which strongly indicated that ClONO and $ClNO_2$ did not react noticeably with HO_2. Poor signal-to-noise prevented similar measurements in the UV.

F. Experimental Uncertainties. The uncertainty (1σ) in the measurement of k' from random noise in the near-IR and UV signals was approximately 2% and 5%, respectively. The uncertainty in the determination of $[NO_2]$ arises from the uncertainty in the accuracy of the NO_2 cross-section[34] and variations in the flow rate of NO_2 into the reaction cell which ranged from 7% at room temperature to 13% at 220 K. The uncertainty in the measured pressure of the reaction cell was approximately 1% and the uncertainty in the temperature was ± 1 K. The uncertainty in methanol concentration was due to uncertainties in the measured flow of carrier gas, pressure above the liquid methanol, temperature of the liquid methanol, and accuracy of the tabulated methanol vapor pressure. The average quadrature sum of these uncertainties was approximately 8%.

III. Results and Discussion

Measurements of the observed rate constants for reaction 1 were obtained using the near-IR probe to monitor HO_2 and the UV probe to measure $[NO_2]$ inside the reaction cell. Experiments were carried out over the temperature range 220−298 K and pressure range 40−200 Torr of N_2 diluent using pseudo first-order conditions ($[NO_2]_o/[HO_2]_o > 30$). All of the kinetics studies used the $Cl_2-CH_3OH-O_2$ mechanism as the source of HO_2 radicals.

As discussed below, we found that methanol enhanced the observed rate of the $HO_2 + NO_2$ reaction due to a chaperone effect involving an HO_2−methanol complex. This effect was particularly evident at low temperatures and high methanol concentrations. A procedure was developed to correct the observed rate constants for methanol at each temperature and pressure. This procedure exploited the fact that the enhancement of k_1 was linearly dependent on $[CH_3OH]$ in the range of methanol concentrations used in this study.

In addition, we ran experiments directly comparing the kinetics derived using UV absorption at 220 nm versus near-IR diode laser spectroscopy to detect HO_2. We found large discrepancies in the time-dependent UV absorption signal at $T < 250$ K. We concluded that measurements of HO_2 by 220 nm absorption were strongly affected by the reestablishment of the NO_2/N_2O_4 equilibrium after initial depletion of NO_2 by reaction 1 and photolysis of NO_2 and N_2O_4.

The following sections describe the results of three sets of experiments. In the first set, we measured the pseudo-first-order rate as a function of methanol concentration and extrapolated the rate to zero methanol. By determining the *y*-intercept and slope of these linear extrapolations as functions of NO_2 concentration, we were able to determine k_1 and parametrize the methanol enhancement of reaction 1. In the second set of measurements, we measured the pseudo-first-order rate of $HO_2 + NO_2$ as a function of $[NO_2]$ at relatively low methanol concentration, as in previous studies of reaction 1.[8−10] We then subtracted out the effect of methanol enhancement using the parametrization determined from the first set of measurements. In the third set of experiments, we examined an unexpected time dependence of the UV signal at 231 K and showed that it is due to the reestablishment of equilibrium between NO_2 and N_2O_4. Using UV−visible spectroscopy, we determined the rate of $N_2O_4 + M \rightarrow NO_2 + NO_2$ at 231 K and 100 Torr.

A. Parametrization of the Methanol Enhancement of $HO_2 + NO_2$ and Extrapolations of k_1. For the first set of measurements, the effect of methanol on the overall rate of $HO_2 + NO_2$ was examined at 100 Torr at six different temperatures ranging from 231 to 298 K. At 231 K, additional studies were also conducted at 200 Torr. The decay of HO_2 in the presence of excess NO_2 was measured at 16 to 25 different combinations of $[NO_2]$ and $[CH_3OH]$ at each temperature and pressure using first-order rate analysis.

Plots of the near-IR measurement of $[HO_2]$ versus time at 100 Torr, 231 K, and $[NO_2] = 2.8 \times 10^{15}$ molecules cm^{-3} are shown in Figure 2 for back-to-back experiments in which only the methanol concentration was changed. The figure illustrates that the HO_2 loss rate increased with increasing methanol concentration. The inset in the figure demonstrates that the kinetic decays obeyed first-order kinetics. The maximum signals at each methanol concentration are roughly equal. The first-order rate constant, k', acquired from fitting such decays as in Figure 2 was determined as a function of methanol concentration. The trend of k' with methanol concentration is shown in Figure 3 for experiments conducted at 100 Torr and 231 K. The dependence was observed to be linear and well described by the equation

$$k' = k'_o + k''[CH_3OH] \quad (9)$$

The value of k'_o represents k' at zero methanol. The value of k'' represents the dependence of the measured first-order rate constant on methanol concentration.

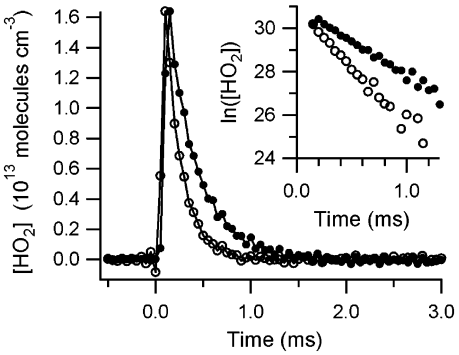

Figure 2. Typical near-IR HO_2 signals at methanol concentrations of 7×10^{14} molecules cm^{-3} (filled circles) and 4×10^{15} molecules cm^{-3} (open circles) at 231 K, 100 Torr, and $[NO_2] = 2.9 \times 10^{15}$ molecules cm^{-3}. The plots shown above are back-to-back experiments in which only the methanol concentration was changed. Time zero is when the excimer laser was fired. The inset is a natural log transform over 3 e^{-1} lifetimes.

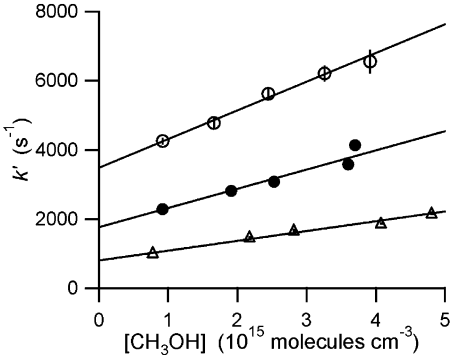

Figure 3. k' versus methanol concentration at 231 K, 100 Torr. The data were acquired at (molecules cm^{-3}) $[NO_2] = 3.7 \times 10^{15}$ (open circles), 1.7×10^{15} (filled circles), and 5.8×10^{14} (open triangles). The *y*-intercept (k'_o) represents k' at zero methanol and the slope (k'') represents the dependence of the measured first-order rate constant on methanol concentration.

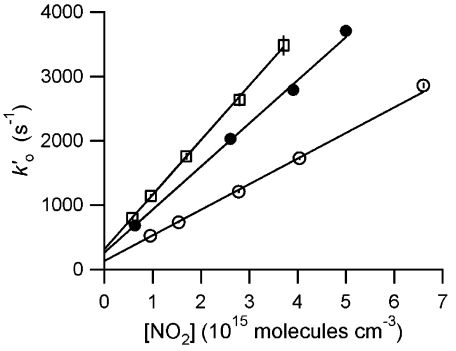

Figure 4. k'_o versus $[NO_2]$ at 100 Torr. The data were acquired at different temperatures: 298 K (open circles), 250 K (filled circles), and 231 K (open squares). The slope of the line is k_1. The *y*-intercept, k'_H, is due to the effect of the HO_2 self-reaction, also at zero methanol, on measurements of k', the observed first-order decay of the IR signal.

Because the HO_2 self-reaction affects k' and because it is enhanced by methanol, both k'_o and k'' had to be correlated with $[NO_2]$ to remove contributions from the HO_2 self-reaction. The relationship between k'_o and $[NO_2]$ is shown in Figure 4 for experiments conducted at 100 Torr and several temperatures. As depicted in the figure, the relationship was linear at all temperatures and thus could be described using the equation

$$k'_o = k'_H + k_1[NO_2] \qquad (10)$$

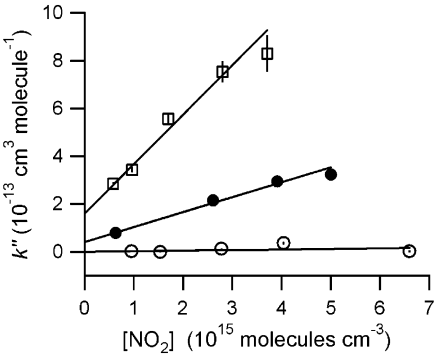

Figure 5. k'' versus $[NO_2]$ at 100 Torr. The data were acquired at different temperatures: 298 K (open circles), 250 K (filled circles), and 231 K (open squares). k'' represents the enhancement in the observed first-order rate due to methanol. The slope, k''', of the fit represents the enhancement of the $HO_2 + NO_2 + M$ reaction due to methanol. The intercept, k''_H, represents the enhancement by methanol of the effect of the HO_2 self-reaction on determinations of k'.

TABLE 3: Measured Rate Coefficients from Studies of Methanol Effect in Which the Methanol Concentration Was Varied—Section III.A

T (K)	*P* (Torr)	k_1[a]	k'''[b]	k_H''[c]
298	100	4.0 ± 0.1	0.24 ± 0.06	not measured
288	100	4.4 ± 0.1	0.58 ± 0.09	0.9 ± 2.0
273	100	5.1 ± 0.1	1.5 ± 0.2	4.5 ± 3.2
250	100	6.7 ± 0.1	6.3 ± 0.2	41 ± 2
240	100	6.9 ± 0.1	13.8 ± 0.4	80 ± 5
231	100	8.5 ± 0.3	20.7 ± 1.4	160 ± 10
231	200	9.4 ± 0.4	23.0 ± 1.9	200 ± 60

[a] In units of 10^{-13} cm^3 $molecule^{-1}$ s^{-1}. [b] In units of 10^{-29} cm^6 $molecule^{-2}$ s^{-1}. [c] In units of 10^{-15} cm^3 $molecule^{-1}$ s^{-1}.

The slope is the rate coefficient for reaction 1. The *y*-intercept, k'_H, is due to the effect of the HO_2 self-reaction on measurements of k'.

The effect of methanol on the overall rate of $HO_2 + NO_2$ was determined by correlating the value of k'' with $[NO_2]$. As illustrated in Figure 5, the trend was linear and thus could be described by the equation

$$k'' = k''_H + k'''[NO_2] \qquad (11)$$

The value of k''' represents the enhancement of the overall rate of $HO_2 + NO_2$ by methanol. The value of k''_H represents the methanol enhancement of the effect due to the HO_2 self-reaction on measurements of k'.

Equations 9, 10, and 11, the result of direct observations, combine to give

$$k' = k'_H + k''_H[CH_3OH] + k_1[NO_2] + k'''[NO_2][CH_3OH] \qquad (12)$$

Following the typical procedure for analysis of pseudo-first-order rate measurements, the overall rate coefficient of $HO_2 + NO_2$, k_{tot}, is

$$\frac{dk''}{d[NO_2]} = k_{tot} = k_1 + k'''[CH_3OH] \qquad (13)$$

Previous studies of the $HO_2 + NO_2$ reaction[8-10] determined k_{tot} rather than k_1 because the effect of methanol was not taken into account.

The temperature dependence of k_1 is tabulated in Table 3 and plotted in Figure 6. As the figure shows, the measured

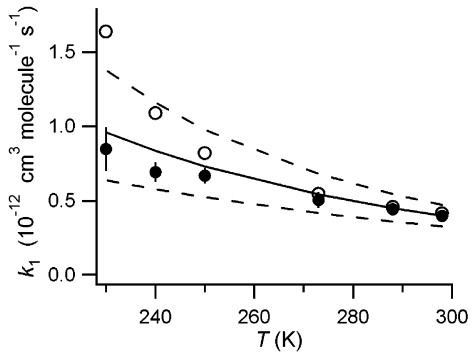

Figure 6. The temperature dependence of k_1 obtained in the present experiment (solid circles) compared with the NASA-recommended values (solid line) at 100 Torr. The dashed lines are the recommended error limits given in the NASA data evaluation. The open circles are calculated overall rate coefficients, k_{tot}, from this study at $[CH_3OH] = 3 \times 10^{15}$ molecules cm^{-3}.

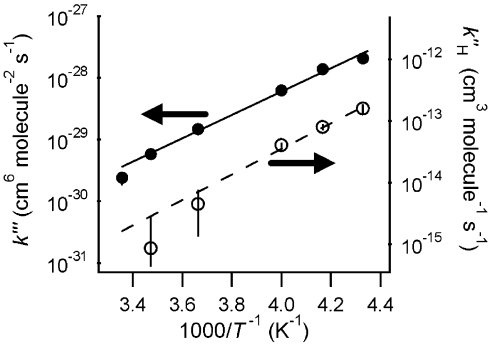

Figure 7. k''' (filled circles) and k''_H (open circles) versus T^{-1}. The value of k''' represents the temperature dependence of the methanol enhancement for the observed rate of $HO_2 + NO_2$. The value of k''_H is a proxy for the effect of methanol on the HO_2 self-reaction (see text). Both *y*-axes range 4 orders of magnitude in order to demonstrate the similarity between their respective temperature dependences.

values of k_1 from this work were within 3% of the NASA recommended values at 298 K and were approximately 15% lower than the recommended values at 231 K. The difference at 298 K is statistically insignificant while the difference at 231 K is within the estimated error limits given in the NASA evaluation.[17]

The temperature dependence of k''' was analyzed using the Arrhenius expression $k(T) = A_o \exp[-E_a/(RT)]$. The value of k''', as a function of temperature, is tabulated in Table 3 and an Arrhenius plot of $\ln(k''')$ versus T^{-1} is shown in Figure 7. The values of A'''_o and E'''_a were found to be $(1.6 \pm 0.9) \times 10^{-36}$ cm^6 molecule^{-2} s^{-1} and (-36.3 ± 1.2) kJ mol^{-1}, respectively. Our measurements at 100 and 200 Torr, as given in Table 3, indicated that k''' was largely pressure independent.

B. Mechanism of Methanol Enhancement. It is likely that enhancement occurs via a chaperone mechanism.[19−23] According to this mechanism, methanol and HO_2 form the hydrogen-bonded adduct $HO_2{\cdot}CH_3OH$. For association reactions, this adduct is more reactive than uncomplexed HO_2 because methanol acts as a third body, removing collisional energy. The observed enhancement of $HO_2 + NO_2$ by methanol can be explained by the following reaction sequence:

$$HO_2 + NO_2 \xrightarrow{M} HO_2NO_2 \qquad (1)$$

$$HO_2 + CH_3OH \rightleftarrows HO_2{\cdot}CH_3OH \qquad (14)$$

$$HO_2{\cdot}CH_3OH + NO_2 \rightarrow \text{products} \qquad (15)$$

Let $K_{eq} = k_{14}/k_{-14}$, the equilibrium constant for the formation of the $HO_2{\cdot}CH_3OH$ complex from HO_2 and methanol. If it is assumed that equilibrium occurs instantaneously compared with reactions 1 and 15, the observed rate coefficient can be described as

$$k_{tot} = \frac{k_1 + k_{15}K_{eq}[CH_3OH]}{1 + K_{eq}[CH_3OH]} \qquad (16)$$

For the present experiment, it was observed that k_{tot} was nearly linear with $[CH_3OH]$, indicating that $\{1 + K_{eq}[CH_3OH]\} \approx 1$ under the conditions of our experiment. Equation 16 can then be simplified to

$$k_{tot} = k_1 + k_{15}K_{eq}[CH_3OH] \qquad (17)$$

This assumption is supported by previous studies of the methanol enhancement of the HO_2 self-reaction,[16,20] and should be valid given the relatively high methanol concentration and the relatively short lifetime of the hydrogen-bonded adduct.

Additional work by our group[35] on the enhancement of the HO_2 self-reaction strongly supports the mechanism outlined above. In that work, we observe the time-dependent decay of the monomer HO_2 concentration (detected by the near-IR laser) as the HO_2 forms the complex and the system approaches equilibrium. Both the forward complexation rate and depletion of free HO_2 are consistent with the chaperone model. We find that the equilibrium between HO_2, CH_3OH, and $HO_2{\cdot}CH_3OH$ is established on the time scale of microseconds. Since the kinetic measurements in the present work are on the order of hundreds of microseconds to milliseconds, the above approximations given in eqs 16 and 17, in which we assume equilibrium between HO_2, CH_3OH, and $HO_2{\cdot}CH_3OH$, are valid.

From eqs 13 and 17, $k''' = k_{15}K_{eq}$; that is, the methanol enhancement rate coefficient is the product of the equilibrium constant and the rate coefficient for the reaction of HO_2 with the complex. If we assume that reaction 15 is temperature independent, a reasonable assumption given that $HO_2 + NO_2$ is exothermic and essentially barrier-less, then the temperature dependence of k''' can be related to the binding energy between methanol and HO_2. Similar assumptions were made in the case of the methanol enhancement of the HO_2 self-reaction.[16,20] In the present case, $\Delta H = (-36.3 \pm 0.3)$ kJ mol^{-1}, which is consistent with a strongly hydrogen-bonded complex.

Though indirect, the temperature dependence of k''_H is a useful proxy for the temperature dependence of the methanol effect on the HO_2 self-reaction. The temperature dependence of k''_H was analyzed using the Arrhenius expression $k(T) = A_o \times \exp[-E_a/(RT)]$. An Arrhenius plot of $\ln(k''_H)$ versus T^{-1} is shown in Figure 7. The values $A''_{H,o}$ and $E''_{H,a}$ were found to be $(1.9 \pm 3.0) \times 10^{-22}$ cm^3 molecule^{-1} s^{-1} and (-39.6 ± 3.1) kJ mol^{-1}, respectively. The activation enthalpies for the enhancements of the $HO_2 + NO_2$ reaction and HO_2 self-reaction should be the same, because the negative temperature dependence for both reactions arises from the rate-limiting formation of the $HO_2{\cdot}CH_3OH$ complex.

The present results are consistent with our previous study of the HO_2 self-reaction.[16] In that study, the rate enhancement was parametrized in the same manner as in this work. From the temperature dependence of the enhancement, ΔH for the formation of the $HO_2{\cdot}CH_3OH$ complex was determined to be (-38.1 ± 2.1) kJ mol^{-1}. The Arrhenius parameters for the methanol enhancement reactions for the $HO_2 + NO_2$ and HO_2 self-reactions are compared in Table 5.

TABLE 4: Measured Rate Coefficients from All Measurements from This Work

T (K)	[M][a]	k_1 [b]	σ[b]	T (K)	[M][a]	k_1 [b]	σ[b]
298[c]	3.24	4.0	0.1	258	1.33	2.9	0.1
295	1.45	2.2	0.1	258	1.67	3.6	0.1
295	1.69	2.5	0.2	258	2.26	4.3	0.1
295	1.97	2.8	0.1	258	2.41	4.5	0.1
295	1.97	2.8	0.1	258	2.99	5.6	0.1
295	2.32	3.2	0.1	258	3.06	5.4	0.1
295	2.66	3.4	0.1	258	3.38	5.7	0.1
295	2.96	3.9	0.2	258	3.66	6.0	0.4
295	3.21	4.1	0.3	258	3.84	6.4	0.1
295	3.54	4.3	0.2	258	4.23	6.4	0.6
295	3.56	4.2	0.2	250[c]	3.86	6.7	0.1
295	3.60	4.2	0.1	243	1.68	4.3	0.3
295	3.62	4.4	0.1	243	2.12	4.9	0.2
295	4.11	4.5	0.1	243	2.97	5.9	0.3
295	4.66	5.0	0.4	243	3.38	6.4	0.2
295	5.01	5.7	0.3	243	3.77	7.6	0.2
295	5.04	5.2	0.2	243	4.05	7.7	0.2
295	5.39	6.1	0.3	243	4.54	8.1	0.3
295	6.36	5.8	0.8	243	4.84	8.5	0.2
288[c]	3.35	4.4	0.1	243	5.41	9.1	0.5
284	1.24	2.1	0.1	243	6.00	9.6	0.3
284	1.75	2.8	0.1	240[c]	4.02	6.9	0.1
284	2.18	3.1	0.1	231[c]	4.17	8.5	0.3
284	2.65	3.6	0.1	231[c]	8.35	9.4	0.4
284	2.89	3.8	0.1	231	1.47	3.7	0.6
284	3.22	4.1	0.1	231	1.68	4.3	0.6
284	3.59	4.4	0.1	231	2.20	5.3	0.6
284	4.09	4.5	0.1	231	2.59	5.5	0.8
284	4.57	5.0	0.2	231	2.73	5.9	0.6
284	4.84	5.0	0.1	231	3.15	6.4	0.6
284	5.21	5.4	0.2	231	3.70	7.4	0.7
273[c]	3.53	5.1	0.1	231	3.84	8.5	0.8
272	1.48	2.6	0.1	231	4.33	8.2	0.8
272	1.98	3.3	0.1	231	4.77	9.5	0.7
272	2.36	3.9	0.1	219	1.57	4.1	0.8
272	2.85	4.3	0.1	219	1.78	4.8	0.9
272	3.21	4.6	0.1	219	2.02	5.3	0.8
272	3.55	5.1	0.1	219	2.44	6.1	0.8
272	3.90	5.4	0.1	219	2.82	6.9	0.9
272	4.31	5.5	0.2	219	3.12	8.2	0.9
272	5.09	5.8	0.1	219	3.28	7.1	0.9
272	5.46	6.5	0.3	219	3.74	8.3	1.0
				219	4.12	8.5	0.9
				219	4.96	9.7	1.0

[a] In units of 10^{18} molecules cm^{-3}. [b] In units of 10^{-13} cm^3 $molecule^{-1}$ s^{-1}. [c] Denotes values from section A.

TABLE 5: Arrhenius Values for k''' and k''_H Compared with the Values from a Previous Study of the HO_2 Self-Reaction

coefficient	A_o	E_a (kJ $mo1^{-1}$)
k'''	$(1.6 \pm 0.9) \times 10^{-36}$ cm^6 $molecule^{-2}$ s^{-1}	-36.3 ± 1.2
k''_H	not applicable	-39.6 ± 3.1
$k'''_{HO_2+HO_2}$[a]	$(2.5 \pm 2.4) \times 10^{-36}$ cm^6 $molecule^{-2}$ s^{-1}	-37.9 ± 1.0

[a] From ref 16. The parametrization used for the HO_2 self-reaction was identical to that used in this work, i.e., the overall rate was a linear function of methanol concentration.

Prior investigators have determined that the equilibrium constant for $HO_2 + H_2O \rightleftarrows HO_2 \cdot H_2O$ may be large enough that at $[H_2O] = 5 \times 10^{15}$ molecules cm^{-3} at 231 K, the ratio of complex to free HO_2 is as large as 0.85.[22] If methanol acts similarly, one might expect that the maximum near-IR signal would decrease with increasing methanol concentration, as more monomer HO_2 becomes bound in the complex due to the equilibrium (reaction 14). In our forthcoming paper,[35] we indeed observe a decrease in the initial HO_2 concentration measured in the near-IR with increasing methanol concentration at low temperatures. In that paper, we determine K_{eq}. Using our estimates of the equilibrium constant, we predict that the ratio of complex to free HO_2 is approximately 0.2 at 231 K and $[CH_3OH] = 4 \times 10^{15}$ molecules cm^{-3}. However, in the present experiment, we find that the initial near-IR HO_2 signal varies little with methanol concentration over the range of methanol concentrations employed in the present experiment. One explanation for this is that the secondary reaction of $Cl + NO_2$ competes with $Cl + CH_3OH$ to suppresses HO_2 formation. This leads to offsetting effects: increasing methanol concentration will increase total HO_2 as more Cl atoms react with CH_3OH, but will decrease free HO_2 due to complexation. As stated above in the Experimental Section, the fraction of Cl atoms reacting with NO_2 as opposed to CH_3OH is 0.2 under the conditions of Figure 3. Due to uncertainties in both the rate of $Cl + NO_2$ and the uncertainty in our measurement of the magnitude of complex formation, it is difficult to predict whether the signal will decrease or increase with CH_3OH.

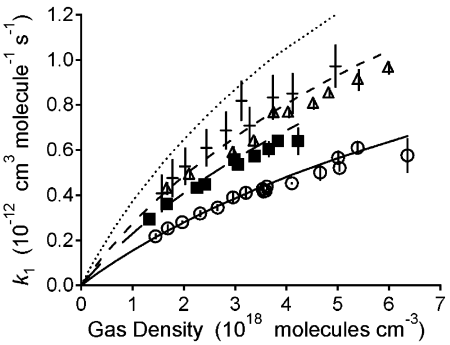

Figure 8. All measured values of k_1 from the present work compared with the NASA-recommended values. Displayed are data acquired at 295 K (open circles), 258 K (solid squares), 243 K (open triangles), and 219 K (horizontal dashes). Also shown are the current NASA recommended values at 295 K (solid line), 258 K (long dashed line), 243 K (medium dashed line), and 219 K (small dashed line).

C. Measurements of k_1 at Low Methanol Concentrations. A more detailed study of reaction 1 was carried out over the temperature range (219−295) K and pressure range (40−200) Torr. In these experiments, a relatively low methanol concentration, $\sim 2.0 \times 10^{14}$ molecules cm^{-3}, was used in order to minimize the methanol enhancement effect on the overall reaction. At this concentration of methanol, the ratio of complex to free HO_2 is expected to be around 0.01.[35]

Using the measured methanol enhancement parameters, k_{tot} was reduced by $k'''[CH_3OH]$ (eq 13). At 100 Torr, this amounted to a reduction in k_{tot} of less than 1% for $T \geq 273$ K and reductions of 4% and 15% at 231 and 219 K, respectively. The measurements of k_1, corrected for the presence of CH_3OH, are shown in Figure 8 for selected temperatures. All measured values of k_1 from the present work are tabulated in Table 4. This includes measurements in which k_1 was obtained by linear extrapolation (section A). There was good agreement between both sets of measurements.

It was assumed that k''' is pressure independent. As described in this work, k''' is the product of pressure independent terms K_{eq} and k_{15} (eq 17). Measurements of k''' at 231 K and different pressures indicate that k''' varies little with pressure over the range of pressures examined in this work, as shown in Table 3. More involved kinetic analysis of the rate enhancement of the HO_2 self-reaction by Mozurkewich and Benson[36] suggests that k''' may display pressure dependence under certain conditions (e.g., very high $[CH_3OH]$ to [M] ratios).

D. Effect of $NO_2 + NO_2 \rightleftarrows N_2O_4$ on Studies of Reaction 1. Previous flash photolysis studies of reaction 1 have used time-

resolved UV absorption spectroscopy as the probe for HO_2.[8−10] In contrast, the present study mainly used the near-IR band. To compare our results with those of previous studies, a number of runs were carried out using simultaneous UV and near-IR detection of HO_2. In these experiments, the monochromator was set to 220 nm. After each run, the monochromator was set to either 369.50 or 381.875 nm to determine [NO_2]. To verify our observations and conclusions, subsequent experiments were conducted with the monochromator set to 400 nm to measure the time dependence of [NO_2].

Comparisons of simultaneously acquired near-IR and UV signals at 100 Torr with the monochromator set at 220 nm are shown in Figures 9a and 9b for 298 and 231 K, respectively. At 298 K, the near-IR and UV signals behaved as predicted. The measured decay rates for both channels were similar. In addition, the residual UV absorption due to the NO_2 absorption background and stable products such as HO_2NO_2 was consistent with the FACSIMILE model. However, at 231 K, there were significant differences between the two channels. The near-IR signal decayed to zero on the order of several milliseconds due to reaction 1, as expected; however, the UV signal showed a time-dependent variation that persisted after the HO_2 was depleted. This variation was not reproduced in the standard model simulations and precluded the determination of k_1 from the UV data when simple first-order rate analysis was employed.

The most likely cause of the unusual behavior in UV signal at low temperatures was transient variations in total absorbance due to changes in [NO_2] and [N_2O_4], both of which have appreciable cross sections at 220 nm and are present in detectable concentrations. The removal of NO_2 by reaction with HO_2 perturbs the equilibrium between NO_2 and N_2O_4. Additionally, photolysis by the excimer beam perturbs the system less significantly. Together, both have the cumulative effect of producing a system in which [NO_2] must increase to reach equilibrium. The time constant for the reestablishment of equilibrium is on the order of milliseconds to tens of milliseconds. This has the effect of decreasing the measured value of k_1.

To support this hypothesis, the time-dependent absorbance was measured at 400 nm. At this wavelength, almost all the absorption is due to NO_2. We detected a transient negative absorbance change ΔA(400 nm) which returned to a negative baseline in the post-HO_2 signal, as shown in Figure 10.

The transient signals at 220 and 400 nm had similar time constants. To model the reestablishment of equilibrium between NO_2 and N_2O_4, first-order analysis of the time dependence of the UV signal at 400 nm was modeled using the reactions listed in Table 2. This wavelength was used because NO_2 can be detected with a high signal-to-noise ratio, and essentially all the observed absorption is due to NO_2. The time interval for the analysis was 5−50 ms after the photolysis pulse. The lower limit was determined by the time required for the HO_2 to decay to background levels, and the upper limit was determined by diffusion and other loss processes. Because K_{eq} for reaction 3 has been measured previously,[17] k_3 was equated to $K_{eq} \cdot k_{-3}$. Thus, the only unknown in the fit was k_{-3}. These fits were done only at 100 Torr and 231 K.

The value of k_{-3} was determined to be (36 ± 10) s^{-1} using the known equilibrium constant. This compares favorably with previous measurements[37] of k_{-3} made at higher temperatures that predict values of k_{-3} between 20 s^{-1} and 180 s^{-1} when extrapolated to 231 K and 100 Torr.

The total absorbance at 220 nm was modeled using FACSIMILE under the conditions of 231 K and 100 Torr. This modeling is shown in Figure 9c. As the figure indicates, the time dependence of the total absorbance replicates that of the experiment shown in Figure 9b. We performed a first-order analysis of the UV rate of decay for experiments conducted at 298 and 231 K in order to ascertain the magnitude of error

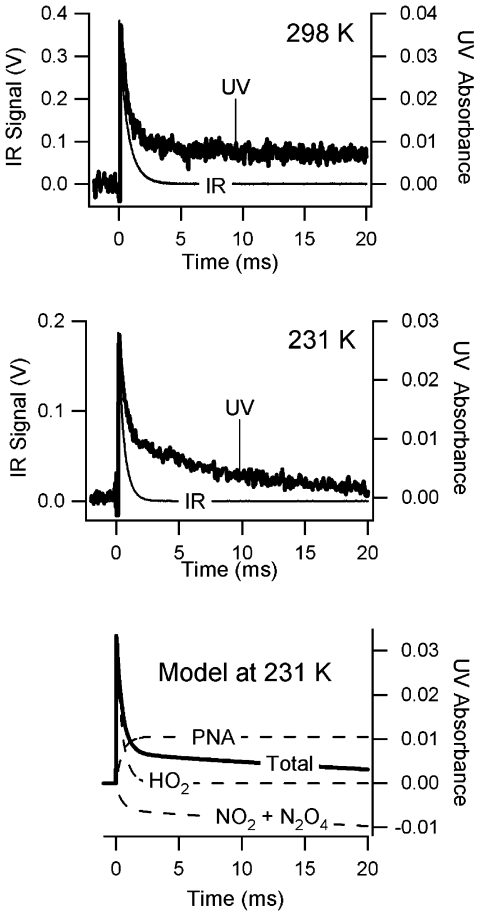

Figure 9. (Top) Comparison of UV and near-IR signals at 298 K. The UV signal was acquired at 220 nm. Note that there is no time dependence in the UV signal after 5 ms. (Middle) Comparison of UV and near-IR signals at 231 K. The UV signal was acquired at 220 nm. Note that there is a time dependence in the UV signal after 5 ms and that the near-IR channel indicates no HO_2 is present. (Bottom) Simulated contributions, at 231 K and 100 Torr, to total UV absorbance at 220 nm using FACSIMILE. Note the time dependence in the total signal after 5 ms, due to combined NO_2 and N_2O_4 absorbance.

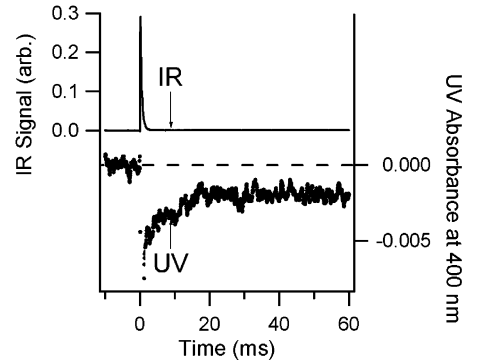

Figure 10. Comparison of simultaneously acquired near-IR and 400 nm signals at 231 K, 100 Torr. Most of the UV absorbance is due to NO_2. Negative absorbance arises from a decrease in [NO_2] which permits more light to arrive at the detector. After the near-IR signal has decreased to zero, at around 5 ms, the UV signal still displays a positive time dependence. This implies that [NO_2] is increasing, most likely from dissociation of N_2O_4.

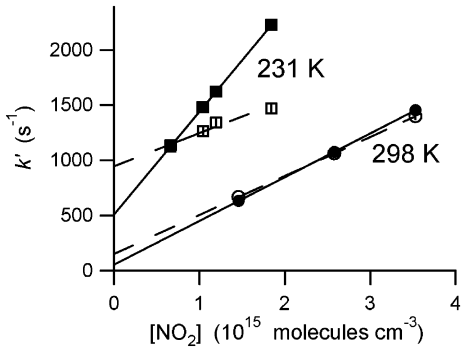

Figure 11. Comparisons of near-IR and UV measurements of the observed rate of $HO_2 + NO_2$ at 231 and 298 K, at 100 Torr and [CH_3OH] = 3×10^{15} molecules cm^{-3}. No correction for the effect of methanol nor the effect of the $NO_2-N_2O_4$ equilibrium has been done. The UV signals were acquired at 220 nm. The near-IR data at 231 and 298 K are solid squares and circles, respectively. The UV data at 231 and 298 K are open squares and circles, respectively.

arising from neglecting the reestablishment of equilibrium between NO_2 and N_2O_4. UV absorbance at 220 nm was employed simultaneously with near-IR detection. Decays were fit over the time period 0−4 ms. Plots of k' versus [NO_2] for both the near-IR and UV data are shown in Figure 11 for 298 and 231 K. At 298 K, the IR and UV measurements agree. At 231 K, they disagree significantly—the slope of the near-IR data is nearly twice that of the UV data at [CH_3OH] = 3×10^{15} molecules cm^{-3}.

We also examined whether the time dependence of the UV signal could be partly attributed to unimolecular decay and/or isomerization of ClONO and $ClNO_2$ since both species absorb appreciably in the UV.[17] We found that the magnitude of this time-dependent signal did not correlate with the wavelength-dependent cross-sections of ClONO and $ClNO_2$ when we scanned our monochromator through the UV at 295 and 231 K. Overall, there was little or no indication of any time dependence in the UV signal that could be attributed to either ClONO and $ClNO_2$.

E. Comparison with Previous Measurements. Our experiments have uncovered two phenomena that affect the apparent rate of reaction 1 at low temperatures—the rate enhancement by methanol, which influences experiments using CH_3OH as a precursor, and the reestablishment of equilibrium between NO_2 and N_2O_4, which leads to artifacts in the UV detection of HO_2. Previous determinations of the rate coefficients for $HO_2 + NO_2$ using the flash photolysis technique neglected both effects. We have found that, independently, these effects lead to significant (>50%) error in the derived rate coefficient k_1. However, as seen in Figure 6, the rate coefficient at 100 Torr obtained in the current work, after correcting for methanol enhancement, is in fair agreement with the recommended values by the NASA Data Evaluation Panel over the temperature range 231 K to 300 K.

This agreement results from a fortuitous cancellation of errors. While studies that used UV to monitor HO_2 appreciably underestimated the rate coefficient of reaction 1 at low temperatures, this error was more than offset by neglect of the enhancement of the $HO_2 + NO_2$ rate by methanol. Overall, the rates at low temperatures recommended by the NASA Data Evaluation Panel based on previous studies appear to be slightly higher than expected had both the reestablishment of $NO_2-N_2O_4$ equilibrium and methanol enhancement been taken into account.

F. Quantifying the Rate Coefficient k_1([M],T). Following the procedure adopted by the NASA data evaluation panel to describe termolecular reactions, a simplified expression for the effective bimolecular rate constant developed by Troe,[38] which here assumes $F_c = 0.6$, was used to quantify k_1 as a function of temperature and pressure:

$$k_1([M],T) = \frac{k_o(T)[M]}{1 + \frac{k_o(T)[M]}{k_\infty(T)}} 0.6^{\{1+[\log(k_o(T)[M]/k_\infty(T))]^2\}^{-1}} \quad (18)$$

The parameters $k_o(T)$ and $k_\infty(T)$ are the low-pressure limit and high-pressure limit rate constants, respectively, with T dependences given by

$$k_o(T) = k_o(300\ K)\cdot(T/300)^{-n} \quad (19)$$

$$k_\infty(T) = k_\infty(300\ K)\cdot(T/300)^{-m} \quad (20)$$

Fitting of data was done over the entire data set of the present work, including values of k_1 that were extrapolated from studies of the methanol enhancement (Section III.A) and those in which the effect of methanol was subtracted out (Section III.C). Values of k_1 at all temperatures and pressures were weighted by the inverse of their uncertainties and fit globally. The results are given in Table 6.

A second, expanded data set was created using the data acquired by Sander and Peterson[8] and Kurylo and Ouellette[9,10] in addition to the present work. Only data for temperatures greater than 276 K were included from the previous studies. We chose this lower temperature limit to prevent inclusion of data in which the effect of methanol enhancement may have affected previous studies. The inclusion of previous work expanded the range of measured values of k_1 to 362 K and 700 Torr. The expanded data set was fit in the same manner as described above and the results are also in Table 6.

As the table illustrates, between the data sets, the values of $k_o(300\ K)$ and n were found to agree within 5% and 10%, respectively. Further, the values of these parameters for both data sets were within the stated uncertainties given in the NASA data evaluation. However, there was significant disagreement between both data sets in regards to the high-pressure rate parameters $k_\infty(300)$ and m. In addition, the values of $k_\infty(300)$ for both data sets were more than 40% lower than the NASA recommended value. Also included in Table 6 are the values measured by Howard[5] using LMR detection of HO_2 between 0.5 and 3 Torr of N_2 at 300 K. The values of $k_o(300\ K)$ determined in the present work, the expanded data set, the NASA recommendation and Howard agree within the stated uncertainties.

Using the NASA recommended values, the pressure at which $k_1 = k_\infty(300)/2$ is greater than 3 atm at 300 K. Thus, the fitted values of $k_\infty(300)$ and m reflect the behavior of the data at these relatively low pressures rather than k_1 at the high-pressure limit. The behavior of the present data that accounts for the lower value of $k_\infty(300)$ is evidenced in Figure 8: the measured values are increasingly smaller than the NASA-recommended values as pressure increases.

The significance of our rate measurements was gauged by examining calculated rates under two different conditions: 200 K, 5 Torr and 230 K, 100 Torr. These conditions are representative of the atmosphere at 40 km and 15 km, respectively. The results are shown in Table 6. There was less than 5% difference between the data set of this work and the expanded data set under both conditions. However, at 200 K, 5 Torr, both data sets predicted values of k_1 that were on average 8% higher than

TABLE 6: Rate Parameters for Reaction 1

data set	k_o (300 K)[a]	n	k_∞ (300 K)[b]	m	k_1[c] 200 K, 5 Torr	k_1[c] 230 K, 100 Torr
this work	2.1 ± 0.1	3.1 ± 0.3	2.4 ± 0.1	1.9 ± 0.5	1.5	8.3
expanded (see text)	2.0 ± 0.1	3.4 ± 0.2	2.9 ± 0.1	1.1 ± 0.3	1.5	8.4
NASA[d]	1.8 ± 0.3	3.2 ± 0.4	4.7 ± 1.0	1.4 ± 1.4	1.4	9.6
Howard[e]	2.1 ± 0.5					

[a] In units of 10^{-31} cm^6 molecule^{-2} s^{-1}, bath gas of N_2. [b] In units of 10^{-12} cm^3 molecule^{-1} s^{-1}. [c] In units of 10^{-13} cm^3 molecule^{-1} s^{-1}. [d] Ref 17. [e] Ref 5.

the NASA-recommended values and at 230 K, 100 Torr, predicted values 15% lower, on average. The latter result is consistent with the observations of this work discussed in Section III.A and shown in Figure 6. It is interesting to note that both data sets predicted values of k_1 which were lower at 230 K, 100 Torr but higher at 200 K, 5 Torr than the NASA recommendation. This is not unexpected given that the latter environmental condition is well removed from any experimental condition investigated and thus greatly extrapolated using eq 18.

The values of k_1 become important for atmospheric chemistry at pressures below 200 Torr and temperatures below 250 K. However, many measurements of k_1 have been acquired at higher pressures and temperatures.[8−10] The question of whether to include data outside the range used for atmospheric modeling then arises. Extrapolations using just the data ($T > 276$ K) acquired by previous researchers to 200 K, 5 Torr and 230 K, 100 Torr are more than 15% and 20% higher than values calculated using just the data from this work, respectively. However, there is little difference in the fitted parameters of eq 18 between the data from this work and the expanded data set, mainly because there are many more data points from the present work. Comparisons with the NASA-recommended values are complicated by the fact that the NASA values have been influenced by measurements in which the contributions of methanol and the $NO_2-N_2O_4$ equilibrium were not taken into account.

IV. Summary and Conclusions

In this study, the temperature and pressure dependences of the rate constant for the $HO_2 + NO_2$ reaction were measured using pulsed laser photolysis with long-path near-IR laser heterodyne detection of HO_2 and in situ detection of NO_2 by long-path visible absorption spectroscopy. The use of the near-IR heterodyne technique for HO_2 detection has a number of advantages over UV detection including improved sensitivity (by at least an order of magnitude) and freedom from spectral interferences since HO_2 is probed via a single rovibronic transition. This eliminated complications encountered in previous studies arising from spectral interferences from the $HO_2 \cdot CH_3OH$ complex, NO_2 and N_2O_4.

Methanol, which was used as a precursor for HO_2, was found to enhance the reaction rate through a chaperone mechanism involving a $HO_2 \cdot CH_3OH$ complex. The $[CH_3OH]$ dependence of the rate constant was measured and used to infer the rate constant of $HO_2 + NO_2$ in the limit of zero methanol. IR spectroscopy was employed, minimizing the influence of the equilibrium between NO_2 and N_2O_4 in determining the rate. Below 250 K, measured k_1 values from the present study were lower than the current NASA recommended values. At 231 K, 100 Torr, k_1 was nearly 15% lower. Parametrizations of the rate of k_1 using a simplified Troe termolecular equation were carried out using the data from this study and previous studies.

The enhancement of reaction 1 by methanol was studied and found to be very similar to that for the methanol enhancement of the HO_2 self-reaction. This validates the chaperone mechanism as the cause of the rate enhancement for reactions involving HO_2.

Measurements of the forward and reverse rates of $NO_2 + NO_2 \rightleftarrows N_2O_4$ were done at 231 K, 100 Torr. The possible effect of the equilibrium between NO_2 and N_2O_4 on previous determinations of k_1 was analyzed.

Acknowledgment. This research was carried out by the Jet Propulsion Laboratory, California Institute of Technology, under contract with the National Aeronautics and Space Administration. This work was supported by the NASA Upper Atmosphere Research and Tropospheric Chemistry Programs and the NASA Graduate Student Researcher Program (GSRP). This research has also been supported in part by a grant from the U.S. Environmental Protection Agency National Center for Environmental Research's Science to Achieve Results (STAR) program, through Grant R826236-01-0. It has not been subjected to any EPA review and therefore does not necessarily reflect the views of the Agency, and no official endorsement should be inferred. We acknowledge the scientific and technical support of Barna László, Dave Natzic, Jürgen Linke, Siamak Forouhar, Dave Dougherty, and Sam Keo of the Jet Propulsion Laboratory.

References and Notes

(1) Simonaitis, R.; Heicklen, J. *J. Phys. Chem.* **1974**, *78*, 653.
(2) Cox, R. A.; Derwent, R. G. *J. Photochem.* **1975**, *4*, 139.
(3) Simonaitis, R.; Heicklen, J. *J. Phys. Chem.* **1976**, *80*, 1.
(4) Niki, H.; Maker, P.; Saveage, C.; Breitenbach, L. *Chem. Phys. Lett.* **1977**, *45*, 564.
(5) Howard, C. J. *J. Chem. Phys.* **1977**, *67*, 5258.
(6) Simonaitis, R.; Heicklen, J. *Int. J. Chem. Kinet.* **1978**, *10*, 67.
(7) Cox, R. A.; Patrick, R. *Int. J. Chem. Kinet.* **1979**, *11*, 635.
(8) Sander, S. P.; Peterson, M. *J. Phys. Chem.* **1984**, *88*, 1566.
(9) Kurylo, M. J.; Ouellette, P. A. *J. Phys. Chem.* **1986**, *90*, 441.
(10) Kurylo, M. J.; Ouellette, P. A. *J. Phys. Chem.* **1987**, *91*, 3365.
(11) Tyndall, G. S.; Orlando, J. J.; Calvert, J. G. *Environ. Sci. Technol.* **1995**, *29*, 202.
(12) WMO. *The Statosphere 1981: Theory and Measurements*; NASA: 1983.
(13) Rinsland, C. P.; Zander, R.; Farmer, C. B.; Norton, R. H.; Brown, L. R.; Russell, J. M.; Park, J. H. *Geophys. Res. Lett.* **1986**, *13*, 761.
(14) Sen, B.; Toon, G. C.; Osterman, G. B.; Blavier, J.-F.; Margitan, J. J. *J. Geophys. Res.—Atmospheres* **1998**, *103*, 3571.
(15) Wennberg, P. O.; Salawitch, R. J.; Donaldson, D. J.; Hanisco, T. F.; Lanzendorf, E. J.; Perkins, K. K.; Lloyd, S. A.; Vaida, V.; Gao, R.; Hintsa, E. J.; Cohen, R. C.; Swartz, W. H.; Kusterer, T. L.; Anderson, D. E. *Geophys. Res. Lett.* **1999**, *26*, 1373.
(16) Christensen, L. E.; Sander, S. P.; Okumura, M.; Salawitch, R. J.; Toon, G. C.; Sen, B.; Blavier, J.-F.; Jucks, K. W. *Geophys. Res. Lett.* **2002**, *29*, art. no. 1299.
(17) Sander, S. P.; Friedl, R. R.; Ravishankara, A. R.; Golden, D. M.; Kolb, C. E.; Kurylo, M. J.; Huie, R. E.; Orkin, V. L.; Molina, L. T.; Moortgat, G. K.; Finlayson-Pitts, B. J. *Chemical Kinetics and Photochemical Data for Use in Atmospheric Studies*; Evaluation No. 14, JPL 02-25, web reference: http://jpldataeval.jpl.nasa.gov; The Jet Propulsion Laboratory: 2003.
(18) Atkinson, R.; Baulch, D. L.; Cox, R. A.; Hampson, R. F., Jr.; Kerr, M. J.; Rossi, M. J.; Troe, J. Evaluated kinetic and photochemical data for atmospheric chemistry: Supplement VI; *J. Phys. Chem. Ref. Data* **1997**, *26*, 1329.
(19) Hamilton, E. J., Jr. *J. Chem. Phys.* **1975**, *63*, 3682.

(20) Andersson, B. Y.; Cox, R. A.; Jenkin, M. E. *Int. J. Chem. Kinet.* **1988**, *20*, 283.
(21) Aloisio, S.; Francisco, J. S. *J. Phys. Chem. A* **1998**, *102*, 1899.
(22) Aloisio, S.; Francisco, J. S.; Friedl, R. R. *J. Phys. Chem.* **2000**, *104*, 6597.
(23) Hamilton, E. J., Jr.; Lii, R.-R. *Int. J. Chem. Kinet.* **1977**, *9*, 875.
(24) Hunziker, H. E.; Wendt, H. R. *J. Chem. Phys.* **1974**, *60*, 4622.
(25) Johnson, T. J.; Wienhold, F. G.; Burrows, J. P.; Harris, G. W.; Burkhard, H. *J. Phys. Chem.* **1991**, *95*, 6499.
(26) Fink, E. H.; Ramsay, D. A. *J. Mol. Spectrosc.* **1997**, *185*, 304.
(27) Taatjes, C. A.; Oh, D. B. *Appl. Opt.* **1997**, *36*, 5817.
(28) Bomse, D. S.; Stanton, A. C.; Silver, J. A. *Appl. Opt.* **1992**, *31*, 718.
(29) Tuckett, R. P.; Freedman, P. A.; Jones, W. J. *Mol. Phys.* **1979**, *37*, 379.
(30) Herriott, D.; Schulte, H. *Appl. Opt.* **1965**, *4*, 883.
(31) Trutna, W.; Byer, R. *Appl. Opt.* **1980**, *19*, 301.
(32) Kircher, C. C.; Sander, S. P. *J. Phys. Chem.* **1984**, *88*, 2082.
(33) Curtis, A. R.; Sweetenham, W. P. *FACSIMILE/CHEKMAT*, H015 ed.; Harwell: Oxfordshire, UK, 1987.
(34) Davidson, J. A.; Cantrell, C. A.; McDaniel, A. H.; Shetter, R. E.; Madronich, S.; Calvert, J. G. *J. Geophys. Res.* **1988**, *93*, 7105.
(35) Christensen, L. E.; Sander, S. P.; Okumura, M.; Francisco, J. S.; Hansen, J. C., Manuscript in preparation.
(36) Mozurkewich, M.; Benson, S. W. *Int. J. Chem. Kinet.* **1985**, *17*, 787.
(37) Markwalder, B.; Gozel, P.; van den Bergh, H. *J. Chem. Phys.* **1992**, *97*, 5472.
(38) Troe, J. *J. Phys. Chem.* **1979**, *83*, 114.
(39) Bass, A. M.; Ledford, A. E.; Laufer, A. H. *J. Res. NBS* **1976**, *80A*, 143.